Strain-induced topological insulator phase transition in HgSe

Lars Winterfeld,[1,2] Luis A. Agapito,[1] Jin Li,[1] Nicholas Kioussis,[1,*] Peter Blaha,[3] and Yong P. Chen[4]
[1]*Department of Physics, California State University, Northridge, California 91330-8268, USA*
[2]*Institut für Physik, University of Technology Ilmenau, 98684 Ilmenau, Germany*
[3]*Institute for Materials Chemistry, TU Vienna, A-1060 Vienna, Austria*
[4]*Department of Physics, Purdue University, West Lafayette, Indiana 47907, USA*
(Received 23 November 2012; revised manuscript received 11 February 2013; published 26 February 2013)

Using *ab initio* electronic structure calculations we investigate the change of the band structure and the ν_0 topological invariant in HgSe (noncentrosymmetric system) under two different types of uniaxial strain along the [001] and [110] directions, respectively. Both compressive [001] and [110] strain lead to the opening of a (crystal field) band gap (with a maximum value of about 37 meV) in the vicinity of Γ, and the concomitant formation of a camel-back- (inverse camel-back-) shaped valence (conduction) band along the direction perpendicular to the strain with a minimum (maximum) at Γ. We find that the $\mathbb{Z}_2$ invariant $\nu_0 = 1$ which demonstrates conclusively that HgSe is a strong topological insulator (TI). With further increase of the strain the band gap decreases, vanishing at a critical strain value (which depends on the strain type) where HgSe undergoes a transition from a strong TI to a trivial (normal) insulator. HgSe exhibits a similar behavior under a tensile [110] uniaxial strain. On the other hand, HgSe remains a normal insulator by applying a [001] tensile uniaxial strain. Complementary electronic structure calculations of the nonpolar (110) surface under compressive [110] tensile strain show two Dirac cones at the Γ point whose spin chiral states are associated with the top and bottom slab surfaces.

DOI: 10.1103/PhysRevB.87.075143 PACS number(s): 71.15.Ap, 72.25.Dc, 73.20.At, 73.43.Nq

I. INTRODUCTION

There has been an explosion of theoretical and experimental research in the search for three-dimensional (3D) topological insulators (TIs), which are a new quantum state of matter with promising applications in spintronics and multifunctional topological-based devices and interfaces.[1,2] TIs are characterized by gapped bulk states, similar to a normal (trivial) insulators, with robust gapless *topologically protected* metallic surface states resulting from the strong spin-orbit coupling (SOC). This in turn leads to an odd number of Dirac-cone-like dispersions crossing the Fermi level at the surface and to a nontrivial $\mathbb{Z}_2$ topological invariant. The surface states exhibit an unconventional spin texture with the spin direction locked to the two-dimensional (2D) electron momentum. Current ongoing research efforts focus primarily on the prototypical single Dirac-cone family of Bi_2Te_3, Bi_2Se_3, and Sb_2Te_3 3D TIs, where angle-resolved photoemission experiments have shown the chiral spin texture of the surface states.[3–5]

Although the band inversion near the time-reversal invariant momenta (TRIM) points ($\vec{k} \equiv -\vec{k} \mod \vec{G}$, where $\vec{G}$ is a reciprocal lattice vector), is a strong indication that a system is TI, it is not definitive because the topological invariant is a global property of the entire occupied Brillouin zone (BZ). Thus, in order to confirm conclusively whether a 3D system is topologically trivial or nontrivial it is essential to compute the $\mathbb{Z}_2$ invariant. For band insulators with crystal inversion symmetry, the topological invariant number can be easily computed as the product of half of the parity (Kramers pairs have identical parities) numbers for all the occupied states at the TRIM points.[6] For the general case of noncentrosymmetric systems (such as zinc-blende structures) the topological invariant can be determined either by integrating both the Berry's connection and curvature over half of the BZ[7] or by calculating the evolution of the Wannier function center during a "time-reversal pumping" process.[8] These two equivalent approaches are discussed in detail in Sec. II.

The mercury chalcogenides HgSe and HgTe in the zinc-blende (ZB) structure belong to a group of unique materials exhibiting the so-called inverted band structure. In this band structure, the energy of the anion *s*-derived Γ_6 state, which is the conduction-band minimum (CBM) at Γ for most ZB semiconductors, is below the anion *p*-like valence-band maximum (VBM) with Γ_8 symmetry. However, the experimental results for the electronic structure of HgSe are controversial. Early photoelectron spectroscopic experiments[9,10] on *n*-type HgSe indicated that this material should have a gap with a positive value for $E_0 \equiv E(\Gamma_6) - E(\Gamma_8) = 0.42$ eV. On the other hand, photoemission experiments[11] of the nonpolar HgSe (110) surface (to minimize the effects of surface charges) could not unequivocally determine the sign of E_0 due to lack of resolution of the sequence of the Γ_6, Γ_7, and Γ_8 bands.

Currently, the consensus of a large amount of experimental results[12] for HgSe seems to give the sequence of the energy bands in ascending order is Γ_6, Γ_7, and Γ_8, with $E_0 \approx -0.2$ eV and the spin-orbit splitting, $\Delta_{SO} \equiv E(\Gamma_8) - E(\Gamma_7) \approx 0.4$ eV. *Ab initio* calculations based on the GW (G is the Green's function and W is the screened Coulomb interaction) scheme find[13–16] $E_0 \approx -0.32$ to -0.58 eV and $\Delta_{SO} \approx 0.27$ to 0.32 eV, in agreement with experiment.

In contrast, in HgTe the sequence of the energy bands is Γ_7, Γ_6, and Γ_8.[13] Interestingly, recent transport experiments[17] on a 70-nm-thick HgTe film, strained by epitaxial growth on a CdTe substrate, show that the strain induces a band gap in the otherwise semimetallic HgTe, rendering it a 3D TI. Similar strain appears when thin HgSe films are epitaxially grown on CdTe or CdSe substrates.

The objective of this work is to investigate the effects of uniaxial strain on the topological phase of HgSe employing *ab initio* calculations. The rest of this paper is organized as

 ©2013 American Physical Society

follows: Section II describes the methodology used to calculate topological invariants and the band structures. In Sec. III we analyze the evolution of the band structure and the topological invariant number under two different types of uniaxial strain along the [001] and [110] directions, respectively. In order to corroborate the topological insulator nature we also present results for the electronic structure of the nonpolar (110) HgSe surface and the spin polarization of the surface states. Finally, conclusions are summarized in Sec. IV.

II. METHODOLOGY

For 2D systems, there are two commonly employed numerical approaches to determine whether a noncentrosymmetric insulator is a TI.

(1) Use the periodic part of the Bloch functions, $|u_n(\vec{k})\rangle$, to calculate the Berry connection, $\vec{A}(\vec{k}) = i\sum_n \langle u_n(\vec{k})|\nabla_{\vec{k}}|u_n(\vec{k})\rangle$, involving the sum over the occupied bands.[7] For a 2D system, both the Berry connection and the Berry curvature, $\mathfrak{F}(\vec{k}) = \nabla_{\vec{k}} \times \vec{A}(\vec{k})$, can then be used to directly compute the topological invariant, z, involving the integration over half of the BZ, denoted by $\mathfrak{B}^+$, i.e.,

$$z = \frac{1}{2\pi}\left[\oint_{\partial\mathfrak{B}^+} \vec{A}(\vec{k})\cdot d\vec{k} - \int_{\mathfrak{B}^+} \mathfrak{F}(\vec{k})d^2k\right] \bmod 2.$$

(2) Employ a recently proposed equivalent method for the $\mathbb{Z}_2$ topological invariant based on the U(2N) non-Abelian Berry connection.[8] This approach allows the identification of the topological nature of a general band insulator without any of the gauge-fixing problems that plague the concrete, previous implementation of invariants. The main idea of the method is to calculate the evolution of the Wannier function center (WFC) directly during a "time-reversal pumping" process, which is a $\mathbb{Z}_2$ analog to the charge polarization proposed by Fu and Kane.[6] The evolution of the WFC along k_y corresponds to the phase factor, θ, of the eigenvalues of the position operator, $\hat{\mathbb{X}}$, projected into the occupied subspace.

Each state of the nth occupied band is indexed by three quantum numbers $|n, k_x, k_y\rangle$. This allows us to define a square matrix $F(k_x,k_y)$ containing the overlap integrals

$$(F(k_x,k_y))_{mn} = \langle m,k_x,k_y|n,k_x + \Delta k_x,k_y\rangle,$$

where $\Delta k_x = \frac{2\pi}{N_x a}$ is the discrete spacing of N_x points. One can in turn calculate the complex unitary square matrix

$$D(k_y) = \prod_{j=0}^{N_x-1} F(j\,\Delta k_x,k_y),$$

which has the complex eigenvalues $\lambda_l(k_y) = |\lambda_l(k_y)|e^{i\theta_l(k_y)}$.

The topological invariant z is then calculated by the even or odd number of crossings of any arbitrary horizontal ($\theta =$ const) reference line with the evolution of the θ_l's, mod 2.

For a 3D bulk system, it is necessary to calculate two different invariants, z_0 and z_π, for the two different BZ planes, $k_z = 0$ and $k_z = \pi$, containing eight TRIM points. The computation for each plane is analogous to the 2D case which has four TRIM points. We employ the second aforementioned approach to calculate the 3D topological invariant, ν_0, which is defined as $\nu_0 \equiv (z_0 - z_\pi) \bmod 2$. The system is in the strong topological insulator (trivial insulator) phase, if ν_0 is 1 (0). More specifically, the system is a nontrivial or strong TI if the evolution curves of the WFC cross an arbitrary reference line an odd number of times in the $k_z = 0$ plane ($z_0 = 1$) and an even number of times in the $k_z = \pi$ plane ($z_\pi = 0$) or vice versa.[8] On the other hand, if the evolution curves cross the arbitrary reference line, an even ($z_0 = z_\pi = 0$) or odd ($z_0 = z_\pi = 1$) number of times in *both* the $k_z = 0$ and $k_z = \pi$ planes, the system is topologically a trivial or normal insulator (NI).

The *ab initio* calculations employed the Vienna Ab initio Simulation Package (VASP) code,[18,19] employing the Perdew-Burke-Ernzerhof (PBE) flavor of the exchange-correlation functional[20] and the projected-augmented-wave approach[21] to represent the electron-ion interaction. The spin-orbit coupling was included in the self-consistent calculations. The Hg 5d electrons are treated explicitly as valence electrons. The energy cutoff of the plane-wave expansion of the basis functions was set to be 550 (450) eV for the bulk (surface) calculations. The BZ integration was performed with a $11 \times 11 \times 11$ ($7 \times 7 \times 1$) **k**-point Monkhorst-Pack mesh[22] for the bulk (surface) calculations. The equilibrium volume, $V_0 = 61.86$ Å^3 per formula unit, is in good agreement with previous *ab initio* calculations.[23] The experimental lattice constant $a = 6.084$ Å [23] differs by 3% from the theoretical equilibrium value of PBE. The nonpolar (110) surface is modeled by a periodic slab consisting of 21 atomic layers with a 12-Å-thick vacuum region separating the periodic slabs.

An accurate description of the electronic structure is a prerequisite in the search and discovery efforts for next-generation TIs. It is known that density functional theory studies[24–26] of TIs based on local or semilocal exchange-correlation functionals can incorrectly predict a material to be a TI when in reality it is not,[27] to the detriment of experiment-theory interplay. This is usually due to the fact that such a local or semilocal treatment systematically underestimates the band gap and can lead to an incorrect ordering of the frontier bands at the TRIM points, which is the determining factor in the prediction of the topological phase. Furthermore, it can also give rise to wrong band topologies and effective masses.[28] Thus, we have also carried out calculations employing the modified Becke-Johnson local density approximation (MBJLDA) method,[29] which predicts[28] band gaps, effective masses, and, most importantly, frontier-band ordering that are in very good agreement with the computationally more intense GW[13] and hybrid-functional[30] approaches.

Figures 1(a) and 1(b) display the PBE and MBJLDA band structures of the undeformed HgSe, respectively, along two symmetry directions, where the MBJLDA parameter $c = 1.2$. PBE predicts the correct level ordering in the upper valence-band region with $E_0 = -1.2$ eV and $\Delta_{SO} = 0.25$ eV, thus yielding a Γ_6 state which is lying far low relative to the Γ_8 state. On the other hand, the MBJLDA shifts the Γ_6 state to a higher energy, resulting in $E_0 = -0.23$ eV and $\Delta_{SO} = 0.20$ eV, in agreement with the values of $E_0 = -0.32$ eV and $\Delta_{SO} = 0.27$ eV of recent GW calculations.[13] The fact that both the PBE and the LDA[13] exchange correlation functionals for HgSe yield the correct frontier band ordering (Γ_7, Γ_8) allows for a reliable determination of the topological invariant.[3] Thus, throughout the remainder of this paper the electronic structure calculations under strain are carried out using the

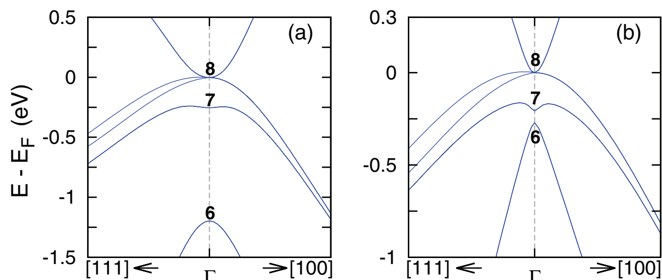

FIG. 1. (Color online) Band structure relative to the Fermi energy of unstrained HgSe along the Γ-X ([100]) and Γ-L ([111]) symmetry directions of the BZ [$\vec{k}_L = \frac{\pi}{a}(1,1,1)$ and $\vec{k}_X = \frac{\pi}{a}(1,0,0)$, where a is the equilibrium lattice constant] calculated by (a) the PBE and (b) the MBJLDA approach,[29] $c_{\rm MBJ} = 1.2$.

PBE exchange correlation functional. The atomic positions were fully relaxed using the conjugate gradient algorithm until all interatomic forces are smaller than 0.01 eV/nm.

III. RESULTS AND DISCUSSION

A. Bulk band structure under uniaxial strain

In order to open a band gap in the semimetallic HgSe, one needs to employ strain. We have carried out calculations under *hydrostatic* pressure in a wide volume range, from -30% to $+30\%$ of the equilibrium volume V_0, in which the equilibrium structure of HgSe remains zinc-blende.[23] We find that within this wide range HgSe always has a zero band gap and, hence, remains a semimetal.

Therefore, we have investigated the evolution of the electronic structure and the topological invariant under *uniaxial* strain, $\epsilon_{[hkl]} \equiv \frac{c-a}{a}$, along the [001] and [110] directions which lowers the T_d symmetry of the ZB structure to D_{2d} and C_{2v}, respectively, and opens a band gap near the Γ point. In both cases, the in-plane lattice constant perpendicular to the strain was fixed to that of the equilibrium ZB structure. Our *ab initio* calculations of the total energy as a function of both uniaxial strains indicate that the corresponding structures are mechanically stable up to strain of ±15%.

1. *[001] strain of D_{2d} symmetry*

Figures 2(a) and 2(b) show the band structures of HgSe under $\epsilon_{[001]}$ of -5% and $+3\%$, respectively, perpendicular to the strain direction. Under a [001] uniaxial tensile (compressive) strain $\epsilon_{[001]} > (<)0$, of D_{2d} symmetry, the half-filled fourfold degenerate Γ_8 state splits into an twofold degenerate occupied valence Γ_{7v} (Γ_{6v}) and a twofold degenerate unoccupied conduction Γ_{6c} (Γ_{7c}) energy levels leading to a positive (negative) splitting, $\Delta^{\Gamma}_{[001]} \equiv E(\Gamma_6) - E(\Gamma_7) > (<)0$.

Under compressive strain ($\Delta^{\Gamma}_{[001]} < 0$) the maxima of the two highest nondegenerate valence bands along the [110] direction, corresponding to the irreducible representations 3 and 4, respectively, occur away from Γ. This gives rise to dumbbell- or camel-back-shaped valence bands with the valence band minima at Γ, due to the fact that band energies along [$\bar{1}\bar{1}0$] (not shown in the figure) are equal to those along [110] due to time-reversal symmetry. Similarly, the Σ_4 conduction band displays a reverse camel-back shape with

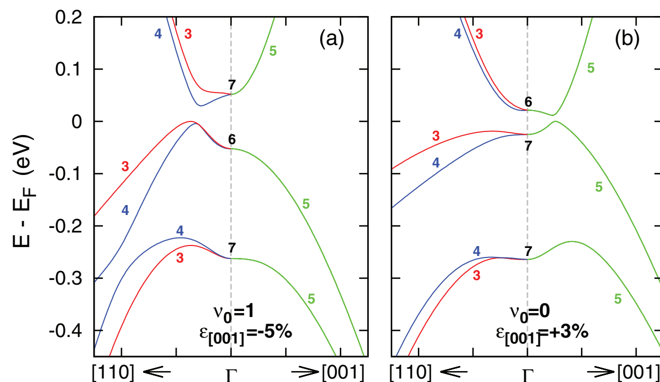

FIG. 2. (Color online) Band structure of HgSe (relative to the Fermi energy E_F) under uniaxial strain along the [001] direction of D_{2d} symmetry near the Γ point along the symmetry directions parallel and perpendicular to the strain direction. (a) The compressive strain of $\epsilon_{[001]} = -5\%$ yields a TI ($\nu_0 = 1$) with $E_{\rm gap} = 37$ meV. (b) The tensile strain of $\epsilon_{[001]} = +3\%$ yields a NI ($\nu_0 = 0$) with $E_{\rm gap} = 13$ meV. Red and blue denote the two spin-polarized bands, while green refers to non-spin-polarized bands.

a maximum at Γ and a minimum along the Σ direction away from Γ. These valence bands along Σ become double degenerate at Γ. This leads to an indirect gap of $E_{\rm gap} = 37$ meV located in a direction perpendicular to the strain axis, in contrast to the case of the [001] tensile stress in Fig. 2(b), where the energy gap $E_{\rm gap}$ occurs along the strain axis.

Figure 2(b) shows the band structure of HgSe under tensile strain of $\epsilon_{[001]} = +3\%$ ($\Delta^{\Gamma}_{[001]} > 0$) along the high symmetry [110] and [001] directions parallel and perpendicular to the strain direction, respectively. Note that along the Δ ([001]) direction of C_{2v} symmetry both the conduction and valence bands are doubly degenerate (denoted by the green curves) of Δ_5 representation. The crystal-field-splitting gap, $E_{\rm gap} =$ 13 meV, which is allowed by the same symmetry of the bands,[31] is observed away from Γ.

2. *[110] strain of C_{2v} symmetry*

Application of uniaxial stress along the [110] reduces the symmetry further to the orthorhombic C_{2v}. As this space group does not allow four-fold-degenerate states, the ZB Γ_8 splits under strain and creates a gap between a valence Γ_{5v} and conduction Γ_{5c}, both of which are twofold degenerate. Under expansion the frontier energy bands exchange their ordering.

Figures 3(a)–3(d) show the evolution of the band structure around Γ, under a uniaxial [110] strain of (a) -5%, (b) $+3\%$, (c) $+6\%$, and (d) $+8\%$, along the [110] ($\hat{x} + \hat{y}$) and [$\bar{1}10$] ($-\hat{x} + \hat{y}$) high $\vec{k}$ symmetry directions, which are parallel and perpendicular to the strain direction, respectively. Under $\epsilon_{[110]} = -5\%$ the direct gap at Γ is $\Delta^{\Gamma}_{[110]} \equiv E(\Gamma_{5c}) - E(\Gamma_{5v}) = 116$ meV. The minimum band gap $E_{\rm gap} = 31$ meV occurs perpendicular to the strain direction between the camel-back-shaped valence and inverse camel-back-shaped conduction bands of Σ_4 irreducible representation.

Figures 4(a) and 4(b) display the evolution of the band gap $E_{\rm gap}$ and the energies of the conduction and valence band states $E(\Gamma_n)$ at Γ as a function of uniaxial strain

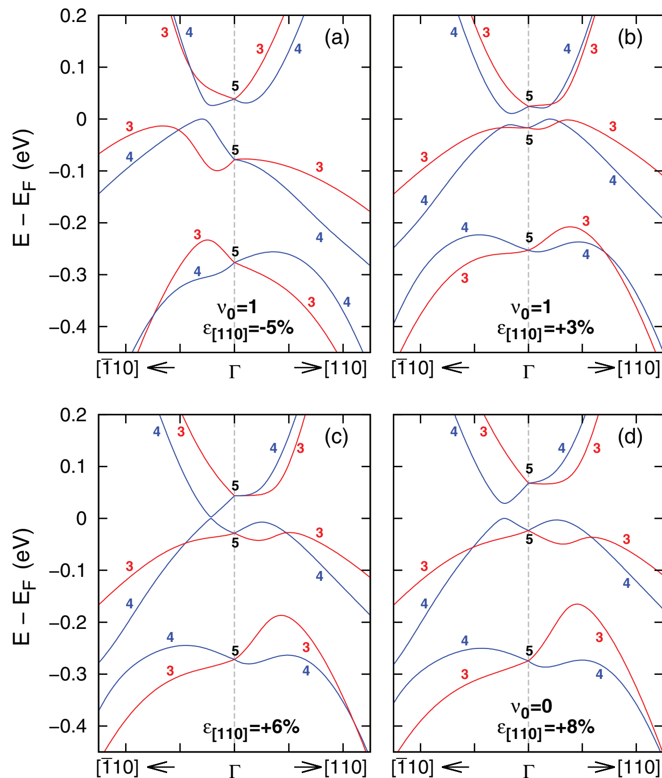

FIG. 3. (Color online) Band structure of HgSe under uniaxial strain along the [110] direction of C_{2v} symmetry near the Γ point along the high symmetry directions parallel and perpendicular to the strain direction. (a) The compressive strain of $\epsilon_{[110]} = -5\%$ yields a TI ($\nu_0 = 1$) with $E_{gap} = 31$ meV. (b) The tensile strain of $\epsilon_{[110]} = +3\%$ yields a TI ($\nu_0 = 1$) with $E_{gap} = 9$ meV. (c) Critical tensile strain $\epsilon_{[110]} = +6\%$ where the conduction and valence bands of irreducible representation 4 cross at E_F and HgSe undergoes a TI ↔ NI transition. (d) At larger tensile strain of $\epsilon_{[110]} = +8\%$ HgSe becomes a NI ($\nu_0 = 0$) with a band gap $E_{gap} = 25$ meV. Red and blue denote the spin-polarized bands.

($-15\% \leqslant \epsilon \leqslant +15\%$) applied along the [001] and [110] directions, respectively. The gray shaded areas denote the strong topological insulating phase with $\nu_0 = 1$, while the white background corresponds to the normal insulating phase ($\nu_0 = 0$). The evolution of ν_0 with uniaxial strain is discussed in more detail in the next section. For [001] strain, the frontier valence and conduction bands at Γ are of Γ_6 and Γ_7 symmetry, while they are of Γ_5 symmetry for the [110] strain. Under both types of uniaxial compression E_{gap} exhibits a nonmonotonic behavior with strain, reaching its maximum value in the topological nontrivial phase ($\nu_0 = 1$) at $\epsilon_{[001]} = -5\%$ and $\epsilon_{[110]} = -6\%$ and vanishing at some critical strain of $\epsilon_{[001]} = -10\%$ and $\epsilon_{[110]} = -13\%$, respectively, where the system undergoes a transition into the trivial insulator phase. On the other hand, HgSe has a different response between [001] and [110] tensile ($\epsilon > 0$) strain. Namely, for $\epsilon_{[001]} > 0$, the band gap is trivial ($\nu_0 = 0$) and increases with strain [Fig. 4(a)], while when $\epsilon_{[110]} > 0$ the system is in a strong topological insulator phase ($\nu_0 = 1$) for $\epsilon_{[110]} \leqslant +5\%$ and it becomes a trivial insulator ($\nu_0 = 0$) at larger strain [Fig. 4(b)].

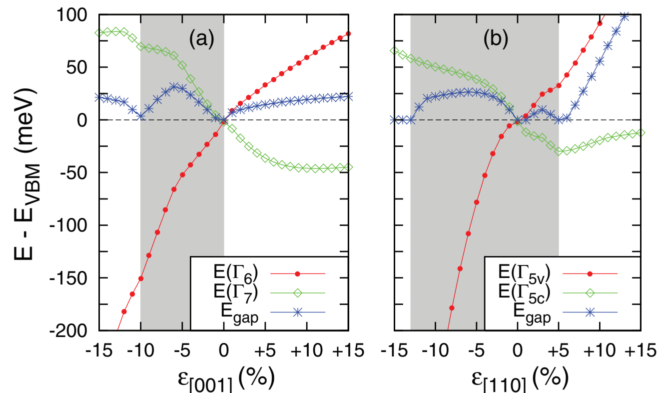

FIG. 4. (Color online) Variation of the band gap E_{gap} and the energies of the conduction band and valence band states, $E(\Gamma_n)$, at the Γ point as a function of uniaxial strain along (a) the [001] direction of D_{2d} symmetry (where $n = 6$ and 7) and (b) the [110] direction of C_{2v} symmetry (where $n = 5c$ and $5v$). The gray shaded areas denote the nontrivial topological phase, where $\nu_0 = 1$.

B. Evolution of topological invariant

An intriguing question is whether there is a correlation between the *change* of the frontier valence and conduction bands and corresponding *changes* in the topological invariant ν_0. Adiabatic deformations of the band structure (not involving band touching or overlaps across the band gap) under external perturbations (such as strain) leave the topology invariant. Murakami[32] has recently studied the classifications of all the possible gap closings in 2D and 3D and showed that the gap closing is associated with the change of the topological invariant number.

In order to elucidate the underlying mechanism of the evolution of both the band inversion and ν_0, we show schematically in Fig. 5 the strain-induced change of the band structure close to the TRIM Γ point along an arbitrary direction (Γ ↔ ±K) in the $k_z = 0$ plane, where the spin-split

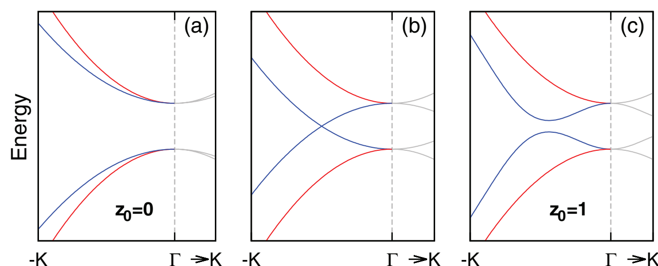

FIG. 5. (Color online) Schematic of the strain-induced evolution of the band structure along an arbitrary direction (Γ ↔ ±K) in the $k_z = 0$ plane where the spin-split bands are denoted by red and blue. (a) The strain splits the originally fourfold degenerate frontier bands at Γ in electron and hole bands which does not involve any band crossing and, hence, the bulk system is in a topologically trivial phase with $z_0 = 0$. (b) Band inversion of one of the spin-split bands (blue) at the critical strain. (c) Odd number (one) of band inversions for one of the bands (blue) at a larger strain, giving rise to a band gap opening away from Γ and the concomitant formation of a camel-back- (inverse-camel-back-) shaped valence (conduction) band along the Γ ↔ ±K direction, rendering the system a strong TI ($z_0 = 1$). Note that the inverted bands exhibit both electron and hole characters.

bands are denoted by red and blue. Figure 5(a) shows that under, for example, a uniaxial tensile strain, the originally four-fold-degenerate Γ_8 state (under zero strain) splits in the spin-polarized electron and hole bands without involving any band inversion. This corresponds to the band structure along the [110] direction for $\epsilon_{[001]} > 0$ in Fig. 2(b). In order to reach the topological phase and its characteristic counterpropagation of opposite spin states (i.e., $\vec{S}_{-\vec{k}} = -\vec{S}_{\vec{k}}$) on the surface, it is necessary to "knot" (entangle) the frontier bands.[33,34] That is achieved by inverting an odd (one) number of spin-split bands (blue) in Fig. 5(b). Further increase of the strain [Fig. 5(c)] gives rise to the opening of a (crystal field) band gap with the concomitant formation of a camel-back- (inverse camel-back-) shape valence (conduction) band along the $\Gamma \leftrightarrow \pm K$ direction. This corresponds to the nondegenerate Σ_4 valence and conduction bands along the [$\bar{1}$10] direction for $\epsilon_{[110]} < 0$ in Fig. 3(a). Since no other band inversions occur along the [110] direction, the system is a strong topological insulator ($z_0 = 1$). Similarly, there is only one band inversion of the valence and conduction bands of Σ_4 character along the [$\bar{1}$10] direction for $\epsilon_{[110]} > 0$ in Fig. 1(b), rendering the system a strong TI. Moreover, the doubly degenerate valence and conduction bands of Δ_5 character along the [001] direction for $\epsilon_{[001]} > 0$ [Fig. 3(b)] have an even (two) number of band inversions and, hence, the system is a topologically a trivial insulator ($z_0 = 0$).

While the above mechanism, based on the changes of the frontier electronic bands (eigenvalues), provides an intuitive explanation of the topological phase transitions, it requires knowledge of the overlap of the 2D conduction and valence energy surfaces. It becomes less practical when these surfaces are not smooth and present multiple extrema. That is the case for Figs. 3(b)–3(d), for instance, requiring a careful examination along multiple $\vec{k}$ directions. For such cases, a less intuitive, but more stringent criterion, is the determination of the topological invariant, $\nu_0 \equiv (z_0 - z_\pi) \bmod 2$, based on the evolution of the Wannier functions (which include a phase factor), as explained in Sec. II. Nonetheless, one notes a clear trend in the evolution of the bands along the [$\bar{1}$10] direction. The gap between the valence and conduction bands of irreducible representation 4 is progressively reduced, with increasing tensile strain, until they cross at ~0 eV for $\epsilon_{[110]} = 5$–6% [Fig. 3(c)]. The system undergoes a second band inversion that "unknots" the band structure. As expected, this closing of the gap coincides with the topological phase transition predicted by the invariant ν_0. For larger strain, this gap increases monotonically [Fig. 3(d)] and without changes to the topological phase.

In HgSe, band inversions occur only in the vicinity of Γ, because the conduction and valence states at other TRIM points are too far separated in energy. Consequently, the bands in the $k_z = \pi$ plane are always not inverted [analogous to Fig. 5(a)] and, hence, $z_\pi = 0$ in the entire strain range, thus yielding $\nu_0 = (z_\pi - z_0 \bmod 2) = z_0$.

Figures 6(a) and 6(b) show the evolution lines of the Wannier centers along k_y in the $k_z = 0$ plane under a uniaxial compression of $\epsilon_{[001]} = -5\%$ and $\epsilon_{[001]} = -15\%$ along the [001] direction, respectively. Under the -5% (-15%) compression the evolution curves (blue) cross any arbitrary line parallel to the horizontal axis (for example, the red dotted line) an odd (even) number of points, thus yielding $z_0 = 1$ ($z_0 = 0$). Furthermore, the evolution lines of the Wannier centers along k_y in the $k_z = \pi$ plane under both uniaxial compression (not shown here) yield $z_\pi = 0$. This demonstrates that under uniaxial compression along [001], there is a topological difference between the TI phase ($\nu_0 = 1$) at $\epsilon_{[001]} = -5\%$ and the trivial insulating phase ($\nu_0 = 0$) at $\epsilon_{[001]} = -15\%$. Interestingly, the critical value of $\epsilon_{[001]} = -10\%$ where HgSe undergoes a TI $\leftrightarrow$ NI transition is close to the critical value of $\epsilon \sim -11\%$, where the ZB structure undergoes a transition to the cinnabar structure.[23] In Figs. 6(c) and 6(d) we show the evolution of the Wannier centers in the $k_z = 0$ plane under a uniaxial compression ($\epsilon_{[110]} = -5\%$) and expansion ($\epsilon_{[110]} = +8\%$) along the [110] direction, where $z_0 = 1$ and $z_0 = 0$, respectively. Since in both cases $z_\pi = 0$, HgSe is a TI ($\nu_0 = 1$) under -5% uniaxial compression while it is in the trivial insulating phase ($\nu_0 = 0$) under 8% uniaxial expansion.

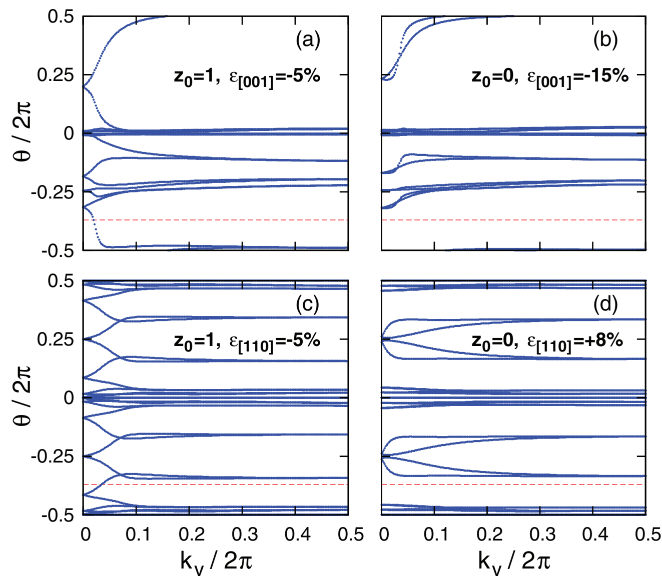

FIG. 6. (Color online) Evolution of Wannier centers for HgSe along k_y in the $k_z = 0$ plane under uniaxial strain along the [001] direction of (a) $\epsilon_{[001]} = -5\%$ and (b) $\epsilon_{[001]} = +15\%$ and along the [110] direction of (c) $\epsilon_{[110]} = -5\%$ and (b) $\epsilon_{[110]} = +8\%$, respectively. The evolution lines cross any arbitrary reference line parallel to k_y (for example, the red dotted line) an odd (even) number of times, yielding $z_0 = 1$ (0). In all cases the corresponding $z_\pi = 0$; $N_x = 48$.

C. Surface band structure and spin polarization

While the $\mathbb{Z}_2$ criterion is sufficient to ascertain whether a 3D bulk system is a TI, an additional commonly employed criterion is the existence of gapless surface states that have spin texture. Therefore, we have carried out electronic structure calculations of the nonpolar (110) HgSe surface to minimize the effects of surface charges and reconstruction associated with polar surfaces. The band structure of a uniaxially strained ($\epsilon_{[110]} = -10\%$) HgSe (110) slab is shown in Fig. 7 along the symmetry directions in the 2D BZ. The states marked in blue are identified to be spatially confined to the top and bottom

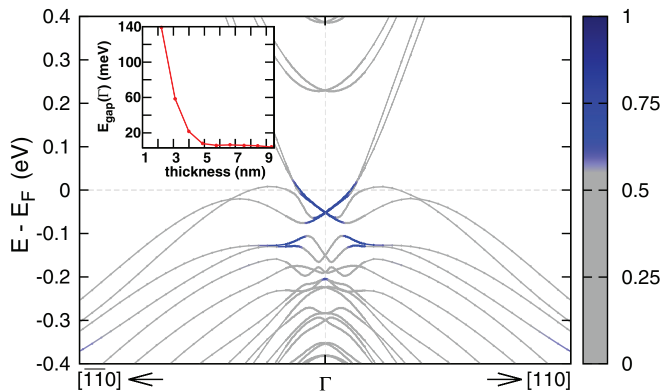

FIG. 7. (Color online) Band structure of the (110) HgSe surface under a [110] uniaxial compressive strain ($\epsilon_{[110]} = -10\%$) along the symmetry directions in the two-dimensional BZ showing a single Dirac cone at Γ at 52 meV below the Fermi energy. The gray and blue bands correspond to bulk- and surface-derived states, where the latter are associated with the two top and bottom atomic layers.[35]

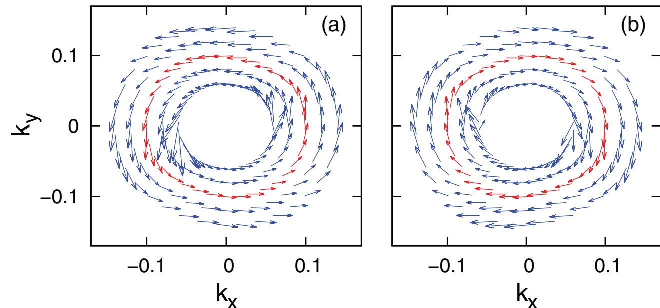

FIG. 8. (Color online) Constant energy contours of surface spin polarization vector of the uniaxially strained (110) HgSe surface in Fig. 7 within an energy of ±25 meV about E_F (all state above the Dirac point), projected onto the (a) top and (b) bottom (011) HgSe surfaces, respectively. The red arrow contours denote the spin polarization vector of states at E_F separating those with energies higher and lower than E_F. The units of k are $2\pi/a$.

boundary layers of the slab, i.e., surface states, using the approach of Park *et al.*[35] The 21-atomic-layer slab exhibits a mirror symmetry with respect to both surfaces. One can clearly see that the topological surface states form two superimposed Dirac cones at the Γ point, each spatially located on the top and bottom surfaces. The Dirac point (52 meV below the Fermi energy) is fourfold degenerate due to Kramer's degeneracy at the TRIM point Γ. The inset shows the variation of the energy gap of the slab at Γ as function of the slab thickness, $D = Na/\sqrt{2}$, where N is the number of atomic layers and $a = 6.278$ Å is the equilibrium lattice constant. The large value of the energy gap in thin slabs is due to the interactions between the states localized at the opposite surfaces. As the number of layers increases, the size of the gap decreases converging to ∼1 meV at the critical thickness of about 7 nm ($N \sim 16$).

Figure 8 shows constant energy contours of the surface spin polarization vector projected on the k_x-k_y plane in the vicinity of the Fermi energy on the top (a) and bottom (b) surface layers, respectively. The red arrow contours denote the spin polarization vector of states at E_F, with the remaining energy contours representing an energy range of ±25 meV about the Fermi energy. We find that $\vec{S}_{-\vec{k}_{||}} \approx -\vec{S}_{\vec{k}_{||}}$ and $\vec{S}_{\vec{k}_{||}}$ is locked almost normal to the in-plane momentum $\vec{k}_{||}$, which results from a combination of the strong SOC and the inversion symmetry breaking at the surface, the well-known Rashba effect.[36] This in turn results in the rotation of the spin orientation around the Fermi surface (spin chirality) as reported for other known TI materials.

IV. CONCLUSIONS

In conclusion, we have investigated the evolution of the band structure and of the topological invariant in HgSe under application of [001] and [110] uniaxial strain. We predict that HgSe is a strong TI ($\nu_0 = 1$) in the compressive strain range, $\epsilon^{cr}_{[001]([110])} \leqslant \epsilon_{[001]([110])} \leqslant 0$, where the (crystal field) band gap occurring away from Γ displays a nonmonotonic strain behavior. The band gap vanishes at $\epsilon^{cr}_{[001]([110])}$, where the system undergoes a TI ↔ NI phase transition. We find that HgSe exhibits a similar behavior applying a [110] tensile strain. On the other hand, under [001] tensile strain HgSe remains a NI. Thus, these calculations demonstrate that HgSe can be tuned into a 3D topological insulator via proper strain engineering.

ACKNOWLEDGMENTS

The research at CSUN was supported by NSF-PREM Grant No. DMR-1205734. Jin Li was supported by a DTRA Grant No. HDTRA1-10-1-0113. Y.P.C. acknowledges support by the DARPA MESO program.

*nick.kioussis@csun.edu

[1] M. Z. Hasan and C. L. Kane, Rev. Mod. Phys. **82**, 3045 (2010).
[2] L. Fu and C. L. Kane, Phys. Rev. B **76**, 045302 (2007).
[3] H. Zhang, C.-X. Liu, X.-L. Qi, X. Dai, Z. Fang, and S.-C. Zhang, Nat. Phys. **5**, 438 (2009).
[4] Y. Xia, D. Qian, D. Hsieh, L. Wray, A. Pal, H. Lin, A. Bansil, D. Grauer, Y. S. Hor, R. J. Cava, and M. Z. Hasan, Nat. Phys. **5**, 398 (2009).
[5] Y. L. Chen, J. G. Analytis, J.-H. Chu, Z. K. Liu, S.-K. Mo, X. L. Qi, H. J. Zhang, D. H. Lu, X. Dai, Z. Fang, S. C. Zhang, I. R. Fisher, Z. Hussain, and Z.-X. Shen, Science **325**, 178 (2009).
[6] L. Fu and C. L. Kane, Phys. Rev. B **74**, 195312 (2006).
[7] T. Fukui and Y. Hatsugai, J. Phys. Soc. Jpn. **76**, 053702 (2007).
[8] R. Yu, X. L. Qi, A. Bernevig, Z. Fang, and X. Dai, Phys. Rev. B **84**, 075119 (2011).
[9] K.-U. Gawlik, L. Kipp, M. Skibowski, N. Orłowski, and R. Manzke, Phys. Rev. Lett. **78**, 3165 (1997).
[10] M. von Truchseß, A. Pfeuffer-Jeschke, C. R. Becker, G. Landwehr, and E. Batke, Phys. Rev. B **61**, 1666 (2000).
[11] C. Janowitz, N. Orlowski, R. Manzke, and Z. Golacki, J. Alloys Compd. **328**, 84 (2001).

[12] S. Einfeldt, F. Goschenhofer, C. R. Becker, and G. Landwehr, Phys. Rev. B **51**, 4915 (1995).
[13] A. Svane, N. E. Christensen, M. Cardona, A. N. Chantis, M. van Schilfgaarde, and T. Kotani, Phys. Rev. B **84**, 205205 (2011).
[14] R. Sakuma, C. Friedrich, T. Miyake, S. Blügel, and F. Aryasetiawan, Phys. Rev. B **84**, 085144 (2011).
[15] A. Fleszar and W. Hanke, Phys. Rev. B **71**, 045207 (2005).
[16] A. Delin, Phys. Rev. B **65**, 153205 (2002).
[17] C. Brüne, C. X. Liu, E. G. Novik, E. M. Hankiewicz, H. Buhmann, Y. L. Chen, X. L. Qi, Z. X. Shen, S. C. Zhang, and L. W. Molenkamp, Phys. Rev. Lett. **106**, 126803 (2011).
[18] G. Kresse and J. Hafner, Phys. Rev. B **47**, 558 (1993).
[19] G. Kresse and J. Furthmüller, Phys. Rev. B **54**, 11169 (1996).
[20] J. P. Perdew, K. Burke, and M. Ernzerhof, Phys. Rev. Lett. **80**, 891 (1998).
[21] P. E. Blöchl, Phys. Rev. B **50**, 17953 (1994).
[22] H. J. Monkhorst and J. D. Pack, Phys. Rev. B **13**, 5188 (1976).
[23] S. Radescu, A. Mujica, J. López-Solano, and R. J. Needs, Phys. Rev. B **83**, 094107 (2011).
[24] D. Xiao, Y. Yao, W. Feng, J. Wen, W. Zhu, X.-Q. Chen, G. M. Stocks, and Z. Zhang, Phys. Rev. Lett. **105**, 096404 (2010).
[25] H. Jin, J.-H. Song, and A. J. Freeman, Phys. Rev. B **83**, 125319 (2011).
[26] W. Feng, W. Zhu, H. H. Weitering, G. M. Stocks, Y. Yao, and D. Xiao, Phys. Rev. B **85**, 195114 (2012).
[27] J. Vidal, X. Zhang, L. Yu, J.-W. Luo, and A. Zunger, Phys. Rev. B **84**, 041109 (2011).
[28] Y.-S. Kim, M. Marsman, G. Kresse, F. Tran, and P. Blaha, Phys. Rev. B **82**, 205212 (2010).
[29] F. Tran and P. Blaha, Phys. Rev. Lett. **102**, 226401 (2009).
[30] J. Heyd, G. E. Scuseria, and M. Ernzerhof, J. Chem. Phys. **118**, 8207 (2003); J. Heyd, J. E. Peralta, G. E. Scuseria, and R. L. Martin, *ibid.* **123**, 174101 (2005).
[31] C.-Y. Moon and S.-H. Wei, Phys. Rev. B **74**, 045205 (2006).
[32] S. Murakami, Physica E **43**, 748 (2011).
[33] C. L. Kane and J. Moore, Phys. World **24**, 32 (2011).
[34] X.-L. Qi and S.-C. Zhang, Phys. Today **63**, 33 (2010).
[35] K. Park, J. J. Heremans, V. W. Scarola, and D. Minic, Phys. Rev. Lett. **105**, 186801 (2010).
[36] É. I. Rashba, Sov. Phys. Solid State **2**, 1109 (1960); Y. A. Bychkov and É. I. Rashba, JETP Lett. **39**, 78 (1984).